Inducible TgfbR1 and Pten deletion in a model of tongue carcinogenesis and chemoprevention

Felipe F Lamenza[1,2], **Nathan M Ryan**[1], **Puja Upadhaya**[1], **Arham Siddiqui**[1], **Pete P Jordanides**[1], **Anna Springer**[1], **Peyton Roth**[1], **Hasan Pracha**[1], **O. Hans Iwenofu**[1], **Steve Oghumu**[1,*]

[1]Department of Pathology, The Ohio State University Wexner Medical Center, Columbus, Ohio, USA.

[2]Department of Microbiology, The Ohio State University, Columbus, Ohio, USA.

Abstract

Head and neck squamous cell carcinoma (HNSCC) is a significant public health problem, with a need for novel approaches to chemoprevention and treatment. Preclinical models that recapitulate molecular alterations that occur in clinical HNSCC patients are needed to better understand molecular and immune mechanisms of HNSCC carcinogenesis, chemoprevention, and efficacy of treatment. We optimized a mouse model of tongue carcinogenesis with discrete quantifiable tumors via conditional deletion of *Tgfβr1* and *Pten* by intralingual injection of tamoxifen. We characterized the localized immune tumor microenvironment, metastasis, systemic immune responses, associated with tongue tumor development. We further determined the efficacy of tongue cancer chemoprevention using dietary administration of black raspberries (BRB). Three Intralingual injections of 500ug tamoxifen to transgenic *K14 Cre*, floxed *Tgfbr1*, *Pten* (2cKO) knock out mice resulted in tongue tumors with histological and molecular profiles, and lymph node metastasis similar to clinical HNSCC tumors. *Bcl2*, *Bcl-xl*, *Egfr*, *Ki-67*, and *Mmp9*, were significantly upregulated in tongue tumors compared to surrounding epithelial tissue. CD4+ and CD8+ T cells in tumor draining lymph nodes and tumors displayed increased surface CTLA4 expression, suggestive of impaired T cell activation and enhanced regulatory T cell activity. BRB administration resulted in reduced tumor growth, enhanced T cell infiltration to the tongue tumor microenvironment and robust anti-tumoral CD8+ cytotoxic T cell activity characterized by greater granzyme B and perforin expression. Our results demonstrate that intralingual injection of tamoxifen in *Tgfβr1/Pten* 2cKO mice results in discrete quantifiable tumors suitable for chemoprevention and therapy of experimental HNSCC.

*Correspondence: Steve Oghumu, PhD, Assistant Professor, Department of Pathology, 249 Evans Hall, 520 King Ave., Columbus, OH 43201, Phone: (614) 685-7556, oghumu.1@osu.edu.

Author Manuscript Author Manuscript Author Manuscript Author Manuscript

Introduction:

Head and neck squamous cell carcinomas (HNSCC), which arise from the tongue, mucosal epithelium of the oral cavity, pharynx, and larynx, accounts for 476,125 new cases and 225,900 deaths worldwide(1, 2). HNSCCs are caused by a diverse range of risk factors which include tobacco consumption, alcohol consumption, exposure to environmental pollutants, and infections from viral agents like the human papilloma virus (HPV)(3, 4). The overall prognosis for patients with HPV-negative HNSCCs is poor, with a current 5-year survival rate ranging from 40 to 50%(5). Existing treatments for HNSCCs are limited to disfiguring surgeries, aggressive radiation, and chemotherapy(4). Significantly, survivors of HNSCC have high rates of suicide due to the psychological distress and compromised quality of life after treatment(6). There is therefore a dire need for increased mechanistic understanding of HNSCC carcinogenesis and novel approaches to HNSCC chemoprevention and therapy.

Preclinical in vivo models for the study of HNSCC include carcinogen induced 4-nitroquinoline 1-oxide (4NQO) administration, orthotopic HNSCC cell line injections, xenograft models into nude mice, and genetically engineered mouse models (GEMM)(7, 8). The well-established 4NQO-induced model of oral squamous cell carcinoma (OSCC) (9, 10) induces genomic alterations that recapitulate the genetic and epigenetic alterations found in tobacco-induced HNSCC carcinogenesis. However, this model takes about 24 weeks to develop, and quantitative measurements of lesion and tumor development can be challenging with this model since tumors can develop in several locations within the oral cavity and gastrointestinal tract. Further, 4NQO-induced HNSCC do not often lead to the development of lymph node and lung metastasis, which are characteristic of human HNSCC (11). Orthotopic injections of HNSCC cell lines for in vivo analysis of tumor growth allows for a quicker experimental timeline and provides for a more robust method to quantify tumor development. This model also develops lymphatic and pulmonary metastasis when metastatic HNSCC cells are used(12, 13). While this is a suitable model for determining HNSCC tumor growth, it does not capture the early stages of HNSCC tumor initiation and progression, which are relevant to the investigation of cancer chemoprevention and early therapeutic strategies. Further, use of immunodeficient mice in some orthotopic models limit investigation of the oral tumor microenvironment which is crucial to HNSCC development and treatment efficacy(13, 14). GEMM models of HNSCC target tissue specific oncogene activation and/or tumor suppressor inactivation of genes known to be associated with HNSCC development (13). These models often utilize the keratin 5 (K5) or keratin 14 (K14) promoter to achieve tissue specific gene mutations in the oral epithelium(7, 15).

Recent advances in the mutational and genetic alteration patterns of HNSCCs have demonstrated frequent alterations in the transforming growth factor-β (TGF- β) and phosphoinositide 3 kinase (PI3K) pathways. These pathways play a major role in metabolism, cell proliferation, survival, apoptosis, and differentiation which contributes to the progression of HNSCC(16, 17). The phosphatase and tensin homolog (PTEN) is a major tumor suppressor of the PI3K pathway that acts to efficiently dephosphorylate the 3' group of phosphatidylinositol (3,4,5)-triphosphate (PIP3) terminating the propagation of the protein kinase B (AKT)(18, 19). Removal of this upstream regulator or acquisition

of oncogenic mutations to overcome negative regulation leads to continuous positive signals, which increase oncogenic potential(18, 20, 21). TGF- β regulates cell proliferation, differentiation, adhesion, migration, and apoptosis(22, 23). TGF- β binding to its receptors TGFBR1 and TGFBR2 lead to SMAD-mediated signaling pathways, but also interacts with other targets including Ras, RhoA, TAK1, MEKK1, PP2A, and PI3K(24, 25). Mice lacking Tgfbr1 display increased cell proliferation and cell survival through the activation of the PI3K pathway, suggesting a crosstalk between the PI3K and TGF- β pathways(26, 27). *Pten* deletion alone does not induce invasive HNSCC in mouse models due to premature senescence by phospho-AKT in the presence of TGF- β. *Tgfbr1* deletion interrupts premature senescence, leading to PI3K mediated development of invasive HNSCC(17).

A recently designed GEMM HNSCC model targeting mutations in the TGFβ and PI3K signaling pathways utilize a tamoxifen inducible Cre-LoxP mediated deletion of *Tgfβr1* and *Pten,* known as *K14-CreER; Tgfβr1$^{flox/flox}$; Pten $^{flox/flox}$* (2cKO) mice(17, 28). Although this model was shown to recapitulate human HNSCC, complete characterization of the immune tumor microenvironment of tumors bearing *TgfbR1* and *Pten* mutations has not been demonstrated. Further, we observed that oral cavity administration (17) of tamoxifen led to variable anatomic lesion manifestations that were challenging to quantify and evaluate efficacy of HNSCC chemoprevention and treatment. To further facilitate the development of discrete quantifiable HNSCC tumors in a localized anatomical site in the mouse oral cavity, we induced the deletion of both the *Tgfβr1* and *Pten* genes by intralingual injection of tamoxifen. Further, we characterized the localized immune tumor microenvironment, systemic immune responses, and lymph node metastasis associated with lesion development due to deregulated TGFB and PI3K signaling during HNSCC carcinogenesis. Finally, to validate this model, we determined the efficacy of HNSCC chemoprevention using dietary black raspberries (*Rubus occidentalis*) (BRBs). Our results demonstrate the utility of our novel approach to the HNSCC GEMM model and provide further insights into mechanisms of BRB associated chemoprevention of HNSCC.

Materials/Methods:

Mice

Tgfβr1$^{flox/flox}$ and *Pten $^{flox/flox}$* knock-in C57BL/6 mice and *K14-CreER^{tam}* transgenic BALB/c mice were obtained from Jackson Laboratories. Sequential rounds of breeding with *Tgfβr1$^{flox/flox}$*, *Pten $^{flox/flox}$* and *K14-CreER^{tam}* resulted in *Tgfβr1/Pten* 2cKO mice (*Tgfβr1$^{flox/}$*lox; Pten *$^{flox/}$*lox; K14-*CreER^{tam+}*) or littermate controls ((*Tgfβr1$^{flox/}$*lox; Pten *$^{flox/}$*lox; K14-*CreER^{tam-}*). Mice were genotyped by PCR analysis of DNA extracted from ear tissue as described previously (29, 30), for the presence of *loxP* sites flanking *Tgfβr1* and *Pten,* and *Cre.* Animals were handled according to regulations maintained by the University Laboratory Animal Resources. Experiments were approved by the Institutional Animal Care and Use Committee (Protocol #2018A00000054) and Institutional Biosafety Committee of The Ohio State University.

Tamoxifen intralingual injections

To conditionally induce deletion of *Pten* and *Tgfβr1* genes, animals were intra-lingually injected using a 27-gauge needle with tamoxifen (Sigma-Aldrich St. Louis, MO, USA), at 500μg and 1000μg in 30μl corn oil (Acros Organics New Jersey, USA), for three or four injections over the course of one week. After 5 weeks, tumor multiplicity and tumor volumes were measured using the formula $V_T = 0.5 \times L \times W^2$ as described previously (31)

Animal diet

Animal diets were prepared as described previously (32). Mice were randomly placed under standardized minimal nutrient rodent chow, AIN-76A (n = 10), or AIN-76A supplemented with 5% black raspberry powder (n = 10) diet. Diets were maintained and food consumption was measured every week throughout the duration of the experiment.

Histology

Tumors and tongues were formalin fixed and paraffin embedded as described previously (32). Tissue sections (5μm) were stained with hematoxylin and eosin. For immunofluorescence and immunohistochemistry, slides were prepared as previously described (32), and stained for Ki-67 (abcam, AB15580-100), TGFβ-R1 (Invitrogen, PA5-32631), PTEN (Cell Signaling, 9559S) cytokeratin (BioLegend, 914202), CD8 (Invitrogen, A21434), and Granzyme B (Cell Signaling, 12653S). Biotinylated goat anti-rabbit (Vector Labs, BA-1000), biotinylated goat anti-mouse (Vector Labs, BA-9200), Alexa Fluor 488-conjugated goat anti-rabbit (Invitrogen, A11034) and Alexa Fluor 555 goat anti-rat (Invitrogen, A21434) were used as secondary antibodies. For immunofluorescence, each tissue was then counterstained with DAPI (BioLegend, San Diego, CA) and confocal imaging was performed using a Zeiss LSM 700 confocal microscope (Carl Zeiss, Munich, Germany). Regions of positive stain were quantified using Image J.

Flow Cytometry

Single cell suspensions were generated from spleens, lymph nodes, tumors and tongues of experimental mice. Cells were stained with fluorochrome-conjugated extracellular antibodies against CD8, CD4, CD49b, PD-1, LAG-3, TIGIT, and CTLA-4. Intracellular staining was performed with antibodies against granzyme B, IFN-γ, TNF-α, IL-2, IL-10 and perforin after stimulation with PMA and ionomycin (BioLegend, San Jose, CA, USA). Samples were analyzed using a FACS Celesta flow cytometer (BD Biosciences; San Jose, CA). Analysis was performed using the FlowJo software (FlowJo; Ashland, OR).

Quantitative Polymerase Chain Reaction

Tongue and tumor samples were lysed with TRIzol. RNA was extracted and cDNA was prepared using a High-Capacity cDNA Reverse Transcription Kit (Applied Biosystems). RT-qPCR was performed on a CFX384 Real-Time PCR system (BioRad; Hercules, CA) using SYBR Green Master Mix (Thermo Fisher; Waltham, MA). Primer sequences for *Ccnd1*, *Id1*, *Bcl2*, *Bcl-xl*, *Egfr*, *Ki-67*, *Mmp9*, and *Nf-κb* were generated using PrimerBank (https://pga.mgh.harvard.edu/primerbank/).

Western Blot

20μg of protein was loaded into a 10% Tris-HCL gel. Proteins were transferred onto polyvinylidene difluoride membranes (0.2μm). Membrane blots were blocked in 5% skim milk for 1 hour and incubated in primary antibody rabbit anti-mouse phospho-AKT (BioLabs 9271S), rabbit anti-mouse PTEN (Cell Signaling, 138G6), rabbit anti-mouse TGFβ-R1 (Thermo Fischer, PA5-32631), rabbit anti-mouse NF-κB (Cell Signaling, 8242S), and mouse anti-mouse BCL-2 (Imgenex, IMG-80093) overnight. Blots were incubated with goat anti-rabbit HRP-linked (31460, Thermo Fisher Scientific, Rockford, IL) and horse anti-mouse HRP-linked (7076S, Cell Signaling) secondary antibodies for 1 hour. Chemiluminescence was detected by ECL Western blotting substrate (ThermoScientific, Waltham, MA). ImageJ was used to quantify the protein intensity.

Statistics

All analysis were conducted and performed in a blinded fashion. Analyses were performed using GraphPad Prism V9.0 (GraphPad Software; San Diego, CA). Student's *t* test (two-sided) was used to determine the statistical significance between the groups.

Results:

Characterization of tamoxifen injected inducible PTEN and TGFβ-R1 knockout mouse

Sequential breeding of *Tgfβr1flox/flox*, *Pten flox/flox*, and *K14-CreERtam* mice resulted in *Tgfβr1flox/flox*; *Pten flox/flox*; *K14-CreERtam* (2cKO) mice displaying Tgfbr1 and Pten deletion upon tamoxifen administration (Fig 1A). We confirmed presence of floxed genes and Cre transgene in 2cKO mice by PCR genotyping (Fig 1B). We also validated tissue specific deletion of Tgfβr1 and Pten after intralingual injection of tamoxifen in the anterior dorsal-lateral area of the mice tongues. We observed little to no expression of *Tgfβr1* and *Pten* genes in the tongue tissues of tamoxifen (tamx+) compared to non-tamoxifen (tamx-) injected 2cKO mice (Fig 1C). Similarly, 2cKO tamx+ mice showed significantly lower levels of Tgfβr1 and Pten protein expression compared to controls (Fig 1D-E). Together, our data demonstrates *Tgfβr1* and *Pten* gene and protein deletion in epithelial tissues of tamoxifen injected 2cKO mice.

Optimization of injection protocol for induction of tongue carcinogenesis in 2cKO mice

In order to achieve localized tumor formation within the oral cavity, as is characteristic of human HNSCC (4), we performed intralingual injections of tamoxifen over a period of one week. Based on previous reports of intralingual tamoxifen injections in a related model of HPV+ mouse HNSCC(33), we tested 3 different tamoxifen injection regimens to determine the optimal dose and frequency that will yield tongue HNSCC tumors, while minimizing toxicity (Figure 2A). Mice were monitored for five weeks after the last tamoxifen injection, and tumor incidence, tumor multiplicity and tumor volume were analyzed at the end of the 5-week period. We observed a 100% incidence of tongue lesion formation at the injection site of all 3 mouse groups tested at day 15 post injection. At the end of the fifth week, all mice developed large HNSCC tumors at the injection site. Secondary and tertiary tumors formed at the opposite site of the injection site and at the tips of the tongues (Fig 2C). No

significant differences in tumor volume and tumor multiplicity were observed between the 3 groups of tamoxifen injection regimens (Figure 2B). Control groups (including (i) 2cKO mice not injected with tamoxifen, (ii) 2cKO mice injected with corn oil vehicle and (iii) floxed *Tgfβr/Pten* without the Cre transgene injected with tamoxifen) did not develop any visible tumors or lesions (Figure 2C). Further H&E histological analysis did not show any lesion development morphology in the control groups (Figure 2D). H&E analysis of the tamoxifen injected mouse groups showed evidence of invasive squamous cell carcinomas, which were similar across all three injection protocols tested (Fig 2D). Based on these results, and to minimize toxicity, we selected three intralingual injections of 500 μg over the course of one week for future studies.

Molecular characterization of tongue tumor development, progression and metastasis in 2cKO mice

Next, we compared the molecular profile of tumors from tamoxifen injected 2cKO mice with established in vivo models of HNSCC as well as with clinical HNSCC patients. We analyzed gene expression patterns of markers commonly altered in human HNSCCs and those found to be upregulated in the 2cKO model from previous studies. *Id1* and *Nfkb*, which were previously found to be upregulated in this model (17), were also significant upregulated compared to heathy tongue epithelial tissue (Figure 3A). *Bcl2*, *Bcl-xl*, *Egfr*, *Ki*-67, and *Mmp9*, genes commonly altered in HNSCCs, and other cancers were also upregulated in tumors of tamoxifen injected 2cKO mice (Figure 3A). We investigated the involvement of the PI3K pathway in molecular alterations associated with HNSCC development in these tumors, given that its negative regulator *Pten* was deleted in 2cKO mice (18, 20, 21). Western blot analysis demonstrated enhanced AKT phosphorylation in tamoxifen injected 2cKO mice compared to controls, suggesting that, similar to human HNSCC, enhanced PI3K signaling activation is associated with tumor development in these mice (Figure 3B). We also confirmed higher protein expression of NF-κB and Bcl2 in tamoxifen injected 2cKO mice compared to controls, further supporting the similarities to human HNSCC (Figure 3B). Next we performed a Ki-67 immunohistochemical staining of tumors and tongues of tamx+ and tamx- mice further corroborated our gene expression data and demonstrated increased tumor cell proliferation in 2cKO mice (Figure 3C).

Lymph node metastasis is a common feature observed in human HNSCC patients, and carcinogen induced models of HNSCC (such as the 4NQO model) does not consistently display lymph node metastatic lesions. We therefore investigated whether tamoxifen injected 2cKO mice more closely mimicked human HNSCC by displaying metastatic lymph nodes. Immunohistological analysis using the HNSCC marker pan-cytokeratin demonstrated metastatic sites in the draining lymph nodes of tamoxifen injected 2cKO but not control mice (Figure 3D). These results demonstrate the utility of intralingual tamoxifen injection of 2cKO mice as a suitable model for investigation of mechanisms of HNSCC invasion and metastasis and determining the efficacy of HNSCC chemoprevention and therapeutic agents.

Tumor associated T cell immune responses of tongue carcinogenesis induced 2cKO mice.

T cells play an important role in tumor immunity and the efficacy of immunotherapeutic strategies against HNSCC. Therefore, we analyzed the T cell immune microenvironment

of tumor bearing 2cKO mice and evaluated their antitumoral properties. Our analysis was initially focused on lymphoid cells in the draining lymph nodes, as this is the site for the initiation of antitumoral immune responses. Similar to what was previously reported, we observed a significantly lower number of CD8+ T cells in the draining lymph nodes of these mice compared to controls, but no differences in CD4+ Tcells and NK cells (Fig 4B-C). We observed CD8+ T cells localized and infiltrating the tongue tumors of the 2cKO mice, indicating the activation of a T-cell response (Fig 4A). Next, we analyzed markers associated with impaired T cell activation, T cell exhaustion and regulatory T cell activity. In both CD4+ and CD8+ T-cells in our tumor bearing 2cKO mice displayed significantly increased levels of CTLA4 expression (Figure 4D), suggestive of impaired T cell activation and enhanced regulatory T cell activity. No differences were found in PD-1 and TIGIT expression within the CD4+ and CD8+ T-cell populations of 2cKO and control mice (Fig 4E and 4G), but we observed lower levels of LAG-3 expressing CD8+ T-cells and CD4+ T-cells in draining lymph nodes of 2cKO mice (Fig 4F).

Next, we examined production of cytokines and effector molecules associated with tumoral immune responses during HNSCC in CD4+, CD8+ and NK cells. We observed higher levels of IFNγ producing CD8+ T-cells and NK cells (Fig 5A), as well as TNFα producing CD8+ T-cells and CD4+ T-cells (Fig 5B) compared to control mice. We found in the lymph nodes, higher levels of CD8+ T-cells producingIL-2 (Fig 5C), while the immunosuppressive cytokine IL-10 was found to be expressed significantly lower in lymph node CD8+ T-cells of cancer bearing mice compared to controls (Fig 5D). Interestingly, while CD8+ T-cells and CD4+ T-cells in the lymoh nodes of tumor bearing 2cKO mice produce higher levels of perforin (Fig 5E), no differences in the levels of granzyme B production were observed in CD8+ T cells of 2cKO mice (Fig 5F). Overall, these results suggest that induction of HNSCC elicits pro- and anti-tumoral immune responses in the draining lymph nodes of 2cKO mice, which can potentially be exploited in immunotherapeutic strategies against HNSCC. Similar analyses were performed on immune cell populations of the spleen, but no major differences were found, suggesting a localized that T cell immune responses to HNSCC tumors in this model (Figs 4 and 5).

Black raspberry diet reduces tongue tumor burdens of mice with PTEN and TGFβ-R1 deletion

To further demonstrate the utility of tamoxifen injected 2cKO model in HNSCC cancer chemoprevention and treatment studies, we evaluated the efficacy of dietary BRB administration on HNSCC development induced by *Pten* and *Tgfbr1* deletion. Previous work by our group and others demonstrates the cancer inhibitory activity of BRB in a 4NQO carcinogen induced model of HNSCC, through mechanisms associated with inhibition of pro-inflammatory, anti-apoptotic and modulation of adaptive immune response pathways (32, 34, 35). We therefore tested whether BRB demonstrated chemopreventive properties in HNSCCs driven by deregulated PI3K and TGFB signaling pathways. Three weeks prior to intralingual tamoxifen injections, 2cKO mice were placed on define AIN-76A diet (control) or AIN-76A supplemented with 5% BRB diet (BRB). Three doses of intralingual tamoxifen injections (500 μg, as determined by our previous studies) were administered to all experimental mice at week 4, and tumor development was monitored for 5 weeks post

tamoxifen injection (Fig 6A). Unlike previous models, HNSCC tumors generated using this model permitted weekly monitoring of tumor size with calipers. Although tumor incidence (100%) was similar between 2cKO mice fed control versus BRB diet, our analysis of tumor sizes demonstrated a reduction in tumor growth in 2cKO mice fed BRB diet compared to 2cKO mice fed control diet (Fig 6B). Similarly, tumor volumes in BRB fed 2cKO mice were significantly reduced compared to 2cKO mice control diet (Fig 6C). This result was corroborated by gross and histological examination of tumors at terminal sacrifice, which revealed significantly smaller tumors in the BRB group compared to the control group (Fig 6D-E). Histologically, tumors from both groups were similar with well to moderately differentiated invasive squamous cell carcinomas. Further, lymph node metastasis was not inhibited by BRB supplemented diet.

Dietary BRB administration promotes T cell infiltration to the tongue tumor microenvironment and stimulates anti-tumoral CD8+ cytotoxic T cell activity.

HNSCC tumors induced by tamoxifen injection of 2cKO mice allow for a more in-depth characterization of immune cells in the tumor microenvironment. Flow cytometric analysis of HNSCC tumors of 2cKO mice demonstrated that BRB administration increased the infiltration of CD4+, CD8+ T-cell and NK cell infiltration to tumors associated with deregulated PI3K and TGFB signaling (Fig 7A-B). We performed an in-depth analysis of these lymphocytes based on immunosuppressive marker expression, and production of tumor associated cytokines and cytotoxic markers. Although BRB administration did not affect the expression level of CTLA-4, PD-1, LAG-3, and TIGIT in the CD4+ and CD8+ T cells in the tumor microenvironment (Supplementary Figure 1), production of IFNγ and IL-2 in CD4+ T-cells and TNFα in CD8+ T-cells were increased in 2cKO mice fed a BRB diet compared to control diet (Fig 7C-E). No effects were observed in IL-10 production by CD4+ and CD8+ T-cells in the tumor microenvironment after BRB administration (Fig 7F). Next, we analyzed the effect of BRB administration on cytotoxic molecule production by CD8+ T cells and NK cells of the tumor microenvironment in 2cKO mice. We observed greater granzyme B and perforin expression by NK cells and greater granzyme B expression in CD8+ T-cells within the tumors of mice fed a BRB diet compared to mice fed a control diet (Fig 8A-C). Together these results indicate that BRB administration promotes T cell infiltration and antitumoral T cell and NK cell responses in HNSCC tumors characterized by deregulated PI3K and TGFB signaling, which contributes to decreased tumor development in 2cKO mice.

Discussion

This study advances the development of oral carcinogenesis GEMM model, which relies on defects in the TGF-β and PI3K/Akt signaling pathways which are commonly altered in human HNSCCs (36). TGF-β provides strong growth inhibitory signals in epithelial cells, and alterations in TGF-β signaling promotes tumorigenesis in some human cancers. Previous reports have shown that deletion of *Tgfbr1* alone is not sufficient for HNSCCs oncogenesis in mice (27). It is likely that cooperation of the TGF-β pathway with other pro-oncogenic pathways is required for malignant transformation in HNSCC. Decreased expression of *Tgfbr1* in mice was associated with activation of the PI3K/Akt pathway

leading to increase cell proliferation and survival (26, 27). Similarly, activation of the PI3K/Akt pathway by genetic deletion the negative regulator *Pten* is not sufficient to cause HNSCC due to the induction of premature senescence induced by phosphorylated Akt in the presence of the tumor suppressor TGF-β (36). Therefore, this model relies on the combined deletion of both *Tgfbr1* and *Pten* to activate the PI3K/Akt pathway and escape premature senescence caused by TGF-β signaling, leading to the development of HNSCC.

Previous work on the *Tgfβr1/Pten* 2cKO mouse model administered tamoxifen for conditional gene deletion via application to the oral cavity, leading to tumor development at different sites within and around the oral cavity (including the ear, skin, and paw) at varying degrees in individual mice. (17, 37). We therefore developed several intralingual injection protocols to explore the possible variations in cancer development between different tamoxifen injection regimens. Our selection of the tongue as a representative organ for experimental HNSCC using this model allows for easy assessment of tumor progression and efficacy of chemopreventive and therapeutic interventions. Further, lesions and tumors in the tongue occur in many cases of human HNSCCs as well as in carcinogen induced mouse models of HNSCC (9, 10). We observed no major differences between the three tamoxifen injection regimens, which led us to proceed with three intralingual injections of 500 μg in 30ul corn oil every other day for 1 week for subsequent experiments.

HNSCC tumors derived from this protocol were very similar pathologically to human HNSCCs and showed similar molecular alterations. The epidermal growth factor receptor (EGFR) is overexpressed in more than 90% of HNSCC cases and in most *in vivo* models (38). Similar upregulation in the proliferation marker Ki-67, the pro-survival markers bcl-2 and bcl-xl, the metalloproteinase 9 (MMP9), and the transcription factor nuclear factor-kappa B (Nf-κb)(39–41), which are common HNSCC cancer progression and associated markers were found to be upregulated in our model.. Furthermore, the transcriptional repressor Id1 was found to be upregulated in our injection protocol tumors. Id1 is negatively regulated downstream of TGF-β signaling, thus deletion of *Tgfβr1* can cause the overexpression of this gene which inactivates the tumor suppressor TP53 (42). TP53 has been found to mediate senescence based on constitutive Akt activity due to PTEN deletion, which we confirmed with high levels of phospho-Akt in the tumors of our mice (43). Senescence in these carcinomas can also be subverted by the inactivation of any member of the p19-p53-p21 pathway, which also work on suppressing the activity of TP53 (44, 45). Our data further confirms the important role Id1 plays in the escape from senescence, which ultimately result in HNSCC tumor development. However, we did not observe a significant upregulation of cyclin D1 (CCND1), which is commonly found to be increased in human and in other mouse models of HNSCC (17, 46). Further exploration of this observation is needed, although other mechanisms associated with the NF-κB signaling pathway may promote HNSCC development and progression in this model(47).

CD4^{+} and CD8^{+} T and NK cells, are the major effector cells in anti-tumoral cell mediated immunity. CD8+ T-cell and NK cell infiltration into the HNSCC tumor microenvironment are essential to promote cancer cell cytotoxicity and are crucial to the success of immune checkpoint inhibitors currently used in HNSCC treatment (48). Our immunological analysis of tumor draining lymph nodes from tumor bearing *Tgfβr1/Pten* 2cKO mice showed CD8+

T-cells expressing higher levels of IFNγ, TNF-α, and the cytotoxic enzyme perforin, while expressing lower levels of the immuno suppressive cytokine IL-10 (49). We also observed a greater level of TNF-α producing CD4+ T-cells, suggesting a Th1 antitumoral phenotype in response to HNSCC tumors (50). Furthermore, increased levels of CTLA-4 expressing T-cells (likely Tregs) were observed in draining lymph nodes of tumor bearing *Tgfβr1/Pten* 2cKO mice which suggests the development of tumor immune escape mechanisms that are typical in patients with HNSCC. The immune response changes were observed in the tumor draining lymph nodes rather than the spleen, indicating a localized immune response to these tumors.

To further demonstrate the utilization of the *Tgfβr1/Pten* 2cKO model for HNSCC chemoprevention studies, we explored mechanisms of HNSCC inhibition by chemopreventive agents in BRB. BRB has been shown to be effective in reducing tumor burdens in oral and aerodigestive cancers. A BRB gel administration resulted in histologic regression and statistically significant reduction in biomarkers of cancer progression (51–53). Our group has previously showed that BRBs modulate Treg and cytotoxic T-cell activity, proinflammatory, glucocorticoid signaling, apoptotic, angiogenic and cell cycle related pathways during HNSCCs chemoprevention, using the 4NQO carcinogen induced model and in vitro experiments (32, 34, 54, 55). Others have also demonstrated similar mechanisms of BRB mediated chemoprevention in other cancers, including esophageal, colorectal, and cervical cancers (56–59). *Tgfβr1/Pten* 2cKO mice fed BRB supplemented diet displayed lower tumor volumes and tongue widths compared to mice receiving a control diet, further supporting chemopreventive ability of BRBs against HNSCCs. BRBs contain numerous bioactive compounds, and the immunological, cellular and biochemical mechanisms underlying BRB mediated HNSCC chemoprevention are not completely understood. Increased recruitment of tumor infiltrating lymphocytes (TILs) to HNSCC tumor microenvironments often correlate with better prognosis and response to treatment (60). BRB diet administration increased the recruitment of TILs to the HNSCC tumor microenvironment. BRB also increased the frequency of IFN-γ and IL-2 producing CD4+ T-cells in HNSCC tumors, cytokines which promote T cell expansion, macrophage activation and cytotoxic CD8+ T-cell activation, which are essential to creating an antitumoral microenvironment (61–63). Increased TNF-α production by CD8+ T-cells of *Tgfβr1/Pten* 2cKO mice fed BRB diet promotes tumor cell cytotoxicity (64), and increased survival outcomes in HNSCC(65, 66). Similar to observations in 4NQO induced mouse model of HNSCC, we demonstrated that that dietary administration of BRB promotes granzyme B production by CD8+ T-cells in the tumor microenvironment of *Tgfβr1/Pten* 2cKO mice(32). These results along with previous reports by our group, indicate an important antitumoral immunomodulatory role of BRB bioactive compounds in HNSCC tumors driven by deregulated PI3K/Akt and TGF-β signaling.

In conclusion, we have developed an optimized protocol for development of easily quantifiable HNSCC tumors using *Tgfβr1/Pten* 2cKO mice. The intralingual tamoxifen injection regimen facilitates the localization of HNSCC tumors, allows for easier quantification, and significantly shortens the experimental timeline. Our analysis of HNSCCs associated biomarkers demonstrates that this approach recapitulates the pathological and molecular characteristics of human HNSCC and other *in vivo* HNSCC

models. We observed the presence of lymph node metastasis and characterized the immune response associated with HNSCC tumors associated with defective PI3K/Akt and TGF-β signaling. Furthermore, using this model, we showed that dietary BRB administration promotes an antitumoral microenvironment characterized by IFN-γ and IL-2 producing CD4^{+} T-cells, and TNF- α and Granzyme B producing CD8^{+} T cells in HNSCC tumors. Future studies will utilize this model to characterize mechanisms of cancer inhibition by chemopreventive or immunotherapeutic agents in HNSCCs initiated by alterations in the TGF-β and PI3K/Akt pathways.

Supplementary Material

Refer to Web version on PubMed Central for supplementary material.

Funding

Data Availability

All data needed to evaluate the conclusions in this paper are present in the article and/or supplementary information. Additional data related to this paper are available from the corresponding author upon reasonable request.

References

1. Sung H, Ferlay J, Siegel RL, Laversanne M, Soerjomataram I, Jemal A, et al. Global Cancer Statistics 2020: GLOBOCAN Estimates of Incidence and Mortality Worldwide for 36 Cancers in 185 Countries. CA Cancer J Clin 2021;71(3):209–49. [PubMed: 33538338]

2. Stein AP, Saha S, Kraninger JL, Swick AD, Yu M, Lambert PF, et al. Prevalence of Human Papillomavirus in Oropharyngeal Cancer: A Systematic Review. Cancer J 2015;21(3):138–46. [PubMed: 26049691]

3. Blot WJ, McLaughlin JK, Winn DM, Austin DF, Greenberg RS, Preston-Martin S, et al. Smoking and drinking in relation to oral and pharyngeal cancer. Cancer Res 1988;48(11):3282–7. [PubMed: 3365707]

4. Johnson DE, Burtness B, Leemans CR, Lui VWY, Bauman JE, Grandis JR. Head and neck squamous cell carcinoma. Nat Rev Dis Primers 2020;6(1):92. [PubMed: 33243986]

5. Sasahira T, Kirita T. Hallmarks of Cancer-Related Newly Prognostic Factors of Oral Squamous Cell Carcinoma. Int J Mol Sci 2018;19(8).

6. Osazuwa-Peters N, Simpson MC, Zhao L, Boakye EA, Olomukoro SI, Deshields T, et al. Suicide risk among cancer survivors: Head and neck versus other cancers. Cancer 2018;124(20):4072–9. [PubMed: 30335190]

7. Ishida K, Tomita H, Nakashima T, Hirata A, Tanaka T, Shibata T, et al. Current mouse models of oral squamous cell carcinoma: Genetic and chemically induced models. Oral Oncol 2017;73:16–20. [PubMed: 28939069]

8. Bais MV, Kukuruzinska M, Trackman PC. Orthotopic non-metastatic and metastatic oral cancer mouse models. Oral Oncol 2015;51(5):476–82. [PubMed: 25682387]

9. Tang XH, Knudsen B, Bemis D, Tickoo S, Gudas LJ. Oral cavity and esophageal carcinogenesis modeled in carcinogen-treated mice. Clin Cancer Res 2004;10(1 Pt 1):301–13. [PubMed: 14734483]

10. Sagheer SH, Whitaker-Menezes D, Han JYS, Curry JM, Martinez-Outschoorn U, Philp NJ. 4NQO induced carcinogenesis: A mouse model for oral squamous cell carcinoma. Methods Cell Biol 2021;163:93–111. [PubMed: 33785171]

11. Vitale-Cross L, Czerninski R, Amornphimoltham P, Patel V, Molinolo AA, Gutkind JS. Chemical carcinogenesis models for evaluating molecular-targeted prevention and treatment of oral cancer. Cancer Prev Res (Phila) 2009;2(5):419–22. [PubMed: 19401522]

12. Myers JN, Holsinger FC, Jasser SA, Bekele BN, Fidler IJ. An orthotopic nude mouse model of oral tongue squamous cell carcinoma. Clin Cancer Res 2002;8(1):293–8. [PubMed: 11801572]

13. Dinesman A, Haughey B, Gates GA, Aufdemorte T, Von Hoff DD. Development of a new in vivo model for head and neck cancer. Otolaryngol Head Neck Surg 1990;103(5 (Pt 1)):766–74. [PubMed: 2126099]

14. Hawkins BL, Heniford BW, Ackermann DM, Leonberger M, Martinez SA, Hendler FJ. 4NQO carcinogenesis: a mouse model of oral cavity squamous cell carcinoma. Head Neck 1994;16(5):424–32. [PubMed: 7960739]

15. Vitale-Cross L, Amornphimoltham P, Fisher G, Molinolo AA, Gutkind JS. Conditional expression of K-ras in an epithelial compartment that includes the stem cells is sufficient to promote squamous cell carcinogenesis. Cancer Res 2004;64(24):8804–7. [PubMed: 15604235]

16. Molinolo AA, Amornphimoltham P, Squarize CH, Castilho RM, Patel V, Gutkind JS. Dysregulated molecular networks in head and neck carcinogenesis. Oral Oncol 2009;45(4–5):324–34. [PubMed: 18805044]

17. Bian Y, Hall B, Sun ZJ, Molinolo A, Chen W, Gutkind JS, et al. Loss of TGF-β signaling and PTEN promotes head and neck squamous cell carcinoma through cellular senescence evasion and cancer-related inflammation. Oncogene 2012;31(28):3322–32. [PubMed: 22037217]

18. Papa A, Pandolfi PP. The PTEN⁻PI3K Axis in Cancer. Biomolecules 2019;9(4).

19. Lee YR, Chen M, Pandolfi PP. The functions and regulation of the PTEN tumour suppressor: new modes and prospects. Nat Rev Mol Cell Biol 2018;19(9):547–62. [PubMed: 29858604]

20. Hollander MC, Blumenthal GM, Dennis PA. PTEN loss in the continuum of common cancers, rare syndromes and mouse models. Nat Rev Cancer 2011;11(4):289–301. [PubMed: 21430697]

21. Fruman DA, Chiu H, Hopkins BD, Bagrodia S, Cantley LC, Abraham RT. The PI3K Pathway in Human Disease. Cell 2017;170(4):605–35. [PubMed: 28802037]

22. Derynck R, Zhang YE. Smad-dependent and Smad-independent pathways in TGF-beta family signalling. Nature 2003;425(6958):577–84. [PubMed: 14534577]

23. Massagué J TGFbeta in Cancer. Cell 2008;134(2):215–30.

24. Moustakas A, Heldin CH. The regulation of TGFbeta signal transduction. Development 2009;136(22):3699–714. [PubMed: 19855013]

25. Zhang YE. Non-Smad pathways in TGF-beta signaling. Cell Res 2009;19(1):128–39. [PubMed: 19114990]

26. Wang J, Yang L, Yang J, Kuropatwinski K, Wang W, Liu XQ, et al. Transforming growth factor beta induces apoptosis through repressing the phosphoinositide 3-kinase/AKT/survivin pathway in colon cancer cells. Cancer Res 2008;68(9):3152–60. [PubMed: 18451140]

27. Bian Y, Terse A, Du J, Hall B, Molinolo A, Zhang P, et al. Progressive tumor formation in mice with conditional deletion of TGF-beta signaling in head and neck epithelia is associated with activation of the PI3K/Akt pathway. Cancer Res 2009;69(14):5918–26. [PubMed: 19584284]

28. Kim H, Kim M, Im SK, Fang S. Mouse Cre-LoxP system: general principles to determine tissue-specific roles of target genes. Lab Anim Res 2018;34(4):147–59. [PubMed: 30671100]

29. Song AJ, Palmiter RD. Detecting and Avoiding Problems When Using the Cre-lox System. Trends Genet 2018;34(5):333–40. [PubMed: 29336844]

30. Leneuve P, Zaoui R, Monget P, Le Bouc Y, Holzenberger M. Genotyping of Cre-lox mice and detection of tissue-specific recombination by multiplex PCR. Biotechniques 2001;31(5):1156–60, 62. [PubMed: 11730022]

31. Ryan N, Anderson K, Volpedo G, Hamza O, Varikuti S, Satoskar AR, et al. STAT1 inhibits T-cell exhaustion and myeloid derived suppressor cell accumulation to promote antitumor immune responses in head and neck squamous cell carcinoma. Int J Cancer 2020;146(6):1717–29. [PubMed: 31709529]

32. Ryan NM, Lamenza FF, Upadhaya P, Pracha H, Springer A, Swingler M, et al. Black raspberry extract inhibits regulatory T-cell activity in a murine model of head and neck squamous cell carcinoma chemoprevention. Front Immunol 2022;13:932742. [PubMed: 36016924]

33. Carper MB, Troutman S, Wagner BL, Byrd KM, Selitsky SR, Parag-Sharma K, et al. An Immunocompetent Mouse Model of HPV16(+) Head and Neck Squamous Cell Carcinoma. Cell Rep 2019;29(6):1660–74.e7. [PubMed: 31693903]

34. Oghumu S, Casto BC, Ahn-Jarvis J, Weghorst LC, Maloney J, Geuy P, et al. Inhibition of Pro-inflammatory and Anti-apoptotic Biomarkers during Experimental Oral Cancer Chemoprevention by Dietary Black Raspberries. Front Immunol 2017;8(1325):1325. [PubMed: 29109723]

35. Knobloch TJ, Uhrig LK, Pearl DK, Casto BC, Warner BM, Clinton SK, et al. Suppression of Proinflammatory and Prosurvival Biomarkers in Oral Cancer Patients Consuming a Black Raspberry Phytochemical-Rich Troche. Cancer Prev Res (Phila) 2016;9(2):159–71. [PubMed: 26701664]

36. Bian Y, Hall B, Sun ZJ, Molinolo A, Chen W, Gutkind JS, et al. Loss of TGF-beta signaling and PTEN promotes head and neck squamous cell carcinoma through cellular senescence evasion and cancer-related inflammation. Oncogene 2012;31(28):3322–32. [PubMed: 22037217]

37. Sun ZJ, Zhang L, Hall B, Bian Y, Gutkind JS, Kulkarni AB. Chemopreventive and chemotherapeutic actions of mTOR inhibitor in genetically defined head and neck squamous cell carcinoma mouse model. Clin Cancer Res 2012;18(19):5304–13. [PubMed: 22859719]

38. Grandis JR, Tweardy DJ. Elevated levels of transforming growth factor alpha and epidermal growth factor receptor messenger RNA are early markers of carcinogenesis in head and neck cancer. Cancer Res 1993;53(15):3579–84. [PubMed: 8339264]

39. Spafford MF, Koeppe J, Pan Z, Archer PG, Meyers AD, Franklin WA. Correlation of tumor markers p53, bcl-2, CD34, CD44H, CD44v6, and Ki-67 with survival and metastasis in laryngeal squamous cell carcinoma. Arch Otolaryngol Head Neck Surg 1996;122(6):627–32. [PubMed: 8639294]

40. Wessely A, Waltera A, Reichert TE, Stöckl S, Grässel S, Bauer RJ. Induction of ALP and MMP9 activity facilitates invasive behavior in heterogeneous human BMSC and HNSCC 3D spheroids. FASEB J 2019;33(11):11884–93. [PubMed: 31366234]

41. Vander Broek R, Snow GE, Chen Z, Van Waes C. Chemoprevention of head and neck squamous cell carcinoma through inhibition of NF-κB signaling. Oral Oncol 2014;50(10):930–41. [PubMed: 24177052]

42. Lee JY, Kang MB, Jang SH, Qian T, Kim HJ, Kim CH, et al. Id-1 activates Akt-mediated Wnt signaling and p27(Kip1) phosphorylation through PTEN inhibition. Oncogene 2009;28(6):824–31. [PubMed: 19079342]

43. Moral M, Segrelles C, Lara MF, Martinez-Cruz AB, Lorz C, Santos M, et al. Akt activation synergizes with Trp53 loss in oral epithelium to produce a novel mouse model for head and neck squamous cell carcinoma. Cancer Res 2009;69(3):1099–108. [PubMed: 19176372]

44. Chen Z, Trotman LC, Shaffer D, Lin HK, Dotan ZA, Niki M, et al. Crucial role of p53-dependent cellular senescence in suppression of Pten-deficient tumorigenesis. Nature 2005;436(7051):725–30. [PubMed: 16079851]

45. Swarbrick A, Roy E, Allen T, Bishop JM. Id1 cooperates with oncogenic Ras to induce metastatic mammary carcinoma by subversion of the cellular senescence response. Proc Natl Acad Sci U S A 2008;105(14):5402–7. [PubMed: 18378907]

46. Loercher A, Lee TL, Ricker JL, Howard A, Geoghegen J, Chen Z, et al. Nuclear factor-kappaB is an important modulator of the altered gene expression profile and malignant phenotype in squamous cell carcinoma. Cancer Res 2004;64(18):6511–23. [PubMed: 15374962]

47. Cohen J, Chen Z, Lu SL, Yang XP, Arun P, Ehsanian R, et al. Attenuated transforming growth factor beta signaling promotes nuclear factor-kappaB activation in head and neck cancer. Cancer Res 2009;69(8):3415–24. [PubMed: 19351843]

48. Raskov H, Orhan A, Christensen JP, Gogenur I. Cytotoxic CD8(+) T cells in cancer and cancer immunotherapy. Br J Cancer 2021;124(2):359–67. [PubMed: 32929195]

49. Kaech SM, Cui W. Transcriptional control of effector and memory CD8+ T cell differentiation. Nat Rev Immunol 2012;12(11):749–61. [PubMed: 23080391]

50. Constant SL, Bottomly K. Induction of Th1 and Th2 CD4+ T cell responses: the alternative approaches. Annu Rev Immunol 1997;15:297–322. [PubMed: 9143690]

51. Shumway BS, Kresty LA, Larsen PE, Zwick JC, Lu B, Fields HW, et al. Effects of a topically applied bioadhesive berry gel on loss of heterozygosity indices in premalignant oral lesions. Clin Cancer Res 2008;14(8):2421–30. [PubMed: 18413833]

52. Mallery SR, Zwick JC, Pei P, Tong M, Larsen PE, Shumway BS, et al. Topical application of a bioadhesive black raspberry gel modulates gene expression and reduces cyclooxygenase 2 protein in human premalignant oral lesions. Cancer Res 2008;68(12):4945–57. [PubMed: 18559542]

53. Mallery SR, Tong M, Shumway BS, Curran AE, Larsen PE, Ness GM, et al. Topical application of a mucoadhesive freeze-dried black raspberry gel induces clinical and histologic regression and reduces loss of heterozygosity events in premalignant oral intraepithelial lesions: results from a multicentered, placebo-controlled clinical trial. Clin Cancer Res 2014;20(7):1910–24. [PubMed: 24486592]

54. Knobloch TJ, Ryan NM, Bruschweiler-Li L, Wang C, Bernier MC, Somogyi A, et al. Metabolic Regulation of Glycolysis and AMP Activated Protein Kinase Pathways during Black Raspberry-Mediated Oral Cancer Chemoprevention. Metabolites 2019;9(7).

55. Nedungadi D, Ryan N, Anderson K, Lamenza FF, Jordanides PP, Swingler MJ, et al. Modulation of the oral glucocorticoid system during black raspberry mediated oral cancer chemoprevention. Carcinogenesis 2022;43(1):28–39. [PubMed: 34888650]

56. Kresty LA, Fromkes JJ, Frankel WL, Hammond CD, Seeram NP, Baird M, et al. A phase I pilot study evaluating the beneficial effects of black raspberries in patients with Barrett's esophagus. Oncotarget 2018;9(82):35356–72. [PubMed: 30450163]

57. Guo J, Yang Z, Zhou H, Yue J, Mu T, Zhang Q, et al. Upregulation of DKK3 by miR-483-3p plays an important role in the chemoprevention of colorectal cancer mediated by black raspberry anthocyanins. Mol Carcinog 2020;59(2):168–78. [PubMed: 31763724]

58. Zhang Z, Knobloch TJ, Seamon LG, Stoner GD, Cohn DE, Paskett ED, et al. A black raspberry extract inhibits proliferation and regulates apoptosis in cervical cancer cells. Gynecol Oncol 2011;123(2):401–6. [PubMed: 21831414]

59. Kresty LA, Frankel WL, Hammond CD, Baird ME, Mele JM, Stoner GD, et al. Transitioning from preclinical to clinical chemopreventive assessments of lyophilized black raspberries: interim results show berries modulate markers of oxidative stress in Barrett's esophagus patients. Nutr Cancer 2006;54(1):148–56. [PubMed: 16800781]

60. Balermpas P, Michel Y, Wagenblast J, Seitz O, Weiss C, Rodel F, et al. Tumour-infiltrating lymphocytes predict response to definitive chemoradiotherapy in head and neck cancer. Br J Cancer 2014;110(2):501–9. [PubMed: 24129245]

61. Geginat J, Paroni M, Facciotti F, Gruarin P, Kastirr I, Caprioli F, et al. The CD4-centered universe of human T cell subsets. Semin Immunol 2013;25(4):252–62. [PubMed: 24183700]

62. Schmitt N, Ueno H. Regulation of human helper T cell subset differentiation by cytokines. Curr Opin Immunol 2015;34:130–6. [PubMed: 25879814]

63. Richardson JR, Schöllhorn A, Gouttefangeas C, Schuhmacher J. CD4+ T Cells: Multitasking Cells in the Duty of Cancer Immunotherapy. Cancers (Basel) 2021;13(4).

64. van Horssen R, Ten Hagen TL, Eggermont AM. TNF-alpha in cancer treatment: molecular insights, antitumor effects, and clinical utility. Oncologist 2006;11(4):397–408. [PubMed: 16614236]

65. Borsetto D, Tomasoni M, Payne K, Polesel J, Deganello A, Bossi P, et al. Prognostic Significance of CD4+ and CD8+ Tumor-Infiltrating Lymphocytes in Head and Neck Squamous Cell Carcinoma: A Meta-Analysis. Cancers (Basel) 2021;13(4).

66. So YK, Byeon SJ, Ku BM, Ko YH, Ahn MJ, Son YI, et al. An increase of CD8. Sci Rep 2020;10(1):20059. [PubMed: 33208791]
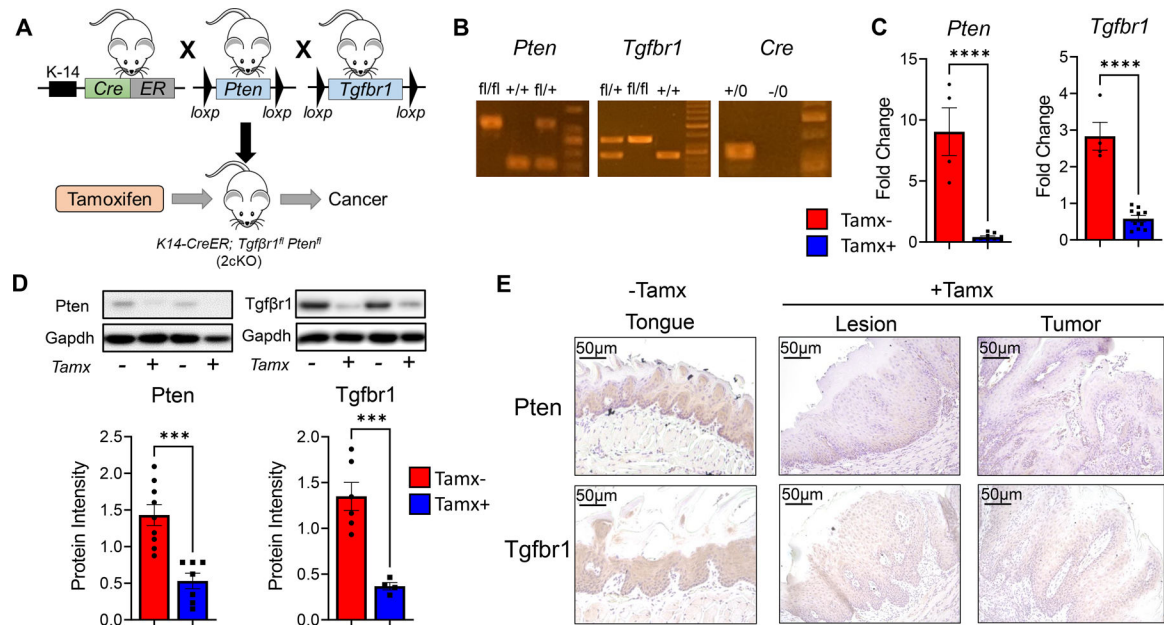
Figure 1: Characterization of tamoxifen injected inducible PTEN and TGFβ-R1 knockout mouse:

(**A**) Strategy for generating *Tgfβr1/Pten* 2cKO mice by sequential breeding of of *Tgfβr1flox/flox*, *Pten flox/flox*, and *K14-CreERtam* mice. HNSCC is induced by intralingual injections of tamoxifen. (**B**) PCR genotyping of *Tgfβr1/Pten* 2cKO mice using Tgfbr1, Pten and K14Cre primers. Respective bands show homozygous floxed (fl/fl) alleles, wild type (+/+) or heterozygous (fl/+) *Pten* and *Tgfβ-r1* genes, and presence (+/0) or absence (-/0) of the *Cre* transgene. (**C**) Gene expression of *Pten* and *Tgfβ-r1* in tongues of *Tgfβr1/Pten* 2cKO mice exposed to tamoxifen (Tamx+) or vehicle control (Tamx-) as determined by RT-qPCR. (**D**) Representative immunoblots and graphical quantification of Pten, Tgfbr1, and Gapdh protein levels in tongues of Tamx+ and Tamx- mice as determined by western blot. (**E**) Representative immunohistochemistry images of tongue tissues (Tamx-) and tumors (Tamx+) of Tgfβr1/Pten 2cKO mice stained with Pten and Tgfbr1 antibodies. Data are presented as mean ± SE *** *P*-value <0.001; **** *P*-value <0.0001.
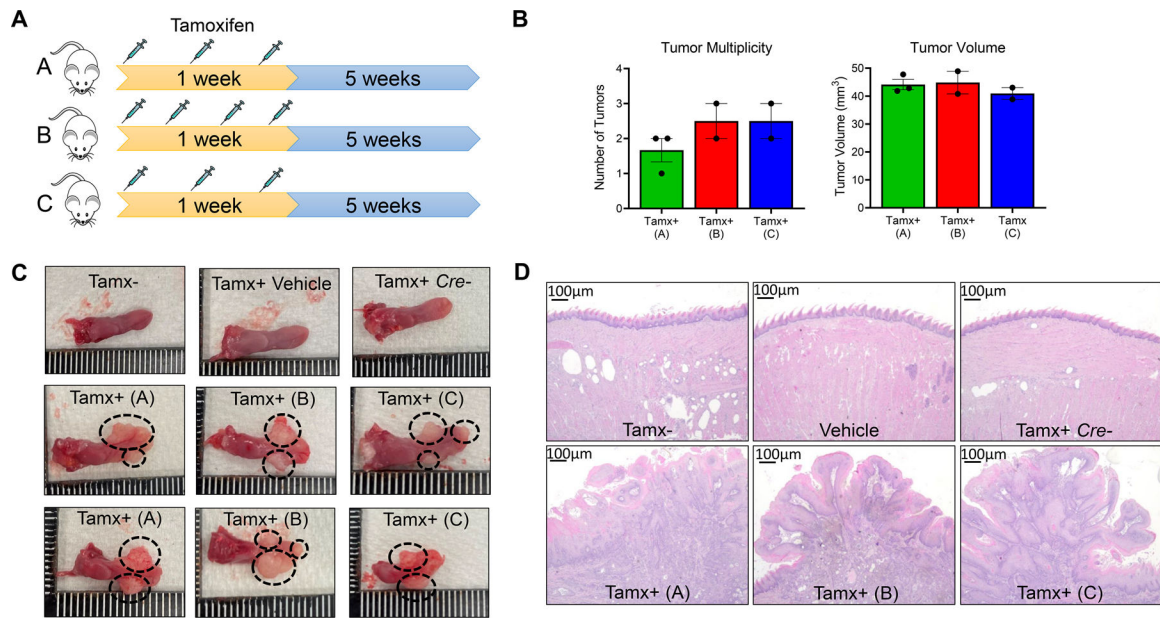
Figure 2: Optimization of injection protocol for induction of HNSCC in *Tgfβr1/Pten* 2cKO mice:
(**A**) Schema of the three intralingual tamoxifen injection regimens tested in *Tgfβr1/Pten* 2cKO mice. (**B**) Counts of tongue tumors and quantification of tumor volumes from *Tgfβr1/Pten* 2cKO mice treated with tamoxifen injection regimens at terminal sacrifice. (**C-D**) (**C**)Representative images of *Tgfβr1/Pten* 2cKO mouse tongues and (**D**) representative H&E-stained images of tongue epithelial tissue from *Tgfβr1/Pten* 2cKO mice treated with different tamoxifen injection regimens or vehicle controls. Tamx-: untreated *Tgfβr1/Pten* 2cKO mice. Vehicle: *Tgfβr1/Pten* 2cKO mice injected with corn oil vehicle. Tamx+ Cre -: *Tgfβr1^{flox/flox}*, *Pten ^{flox/flox}*, *K14Cre^-* (Cre negative control) mice injected with 500 μg tamoxifen. Tamx+ (A) *Tgfβr1/Pten* 2cKO mice injected with 500 μg of tamoxifen for 3 intralingual injections, Tamx+ (B): *Tgfβr1/Pten* 2cKO mice injected with 500 μg of tamoxifen for 4 intralingual injections, Tamx+ (C): *Tgfβr1/Pten* 2cKO mice injected with 1000 μg of tamoxifen for 3 intralingual injections. Tumors are shown with black dotted circles.
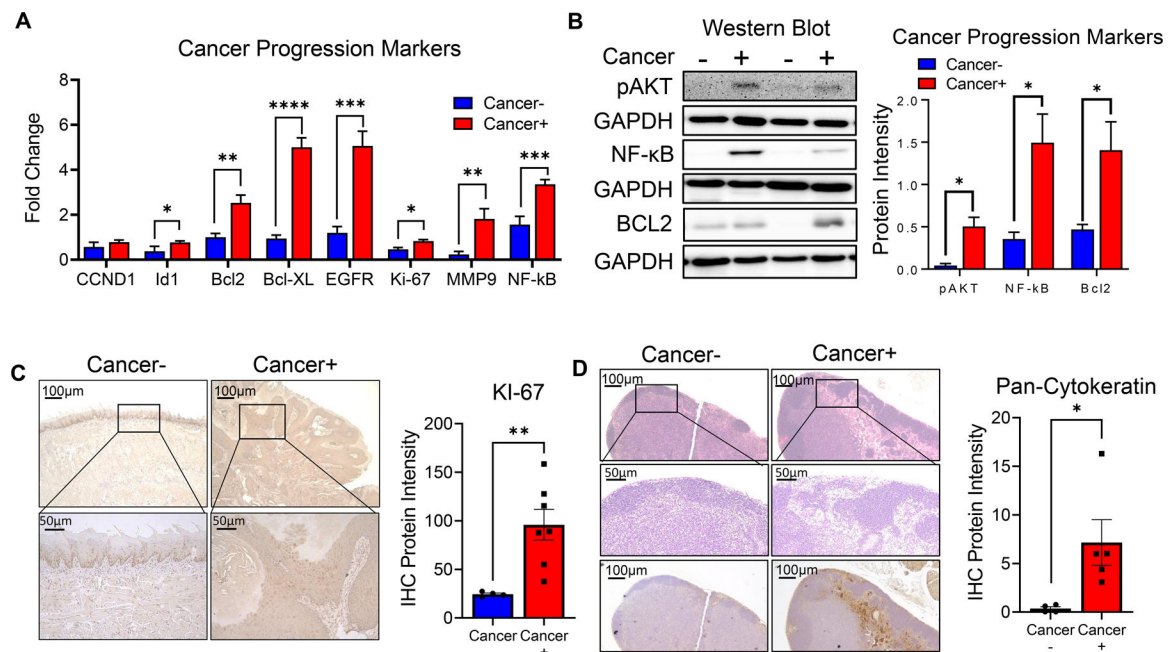
Figure 3: Molecular characterization of HNSCC tumor development, progression, and metastasis in *Tgfβr1/Pten* 2cKO mice:

(**A**) Gene expression of *Ccnd1*, *Id1*, *Bcl2*, *Bcl-xl*, *Egfr*, *Ki-67*, *Mmp9*, and *Nf-κb* at primary tumors or tongue tissues of tumor bearing (cancer+) and non tumor bearing (cancer-) *Tgfβr1/Pten* 2cKO mice as determined by RT-qPCR. (**B**) Representative Western blot images and graphical quantification of phospho-AKT, NF-κB, BCL2, and GAPDH protein levels in tongues of tumor bearing (cancer+) and non-tumor bearing (cancer-) mice. (**C**) Representative immunohistochemistry images of primary tumors or tongue tissues of tumor bearing (cancer+) and non tumor bearing (cancer-) *Tgfβr1/Pten* 2cKO mice stained with KI-67 antibody. Bar graphs depict regions of positive staining taken from at least three fields with $N = 4$–7 animals per group.

(**D**) Representative H&E and immunohistochemistry (pan-cytokeratin) images of tumor draining lymph nodes of tumor bearing (cancer+) and non tumor bearing (cancer-) *Tgfβr1/Pten* 2cKO mice. Bar graphs depict regions of pan-cytokeratin positive staining taken from at least three fields with $N = 4$–5 animals per group. Data are presented as mean ± SE * P-value < 0.05; ** P-value < 0.01; *** P-value <0.001; **** P-value <0.0001.
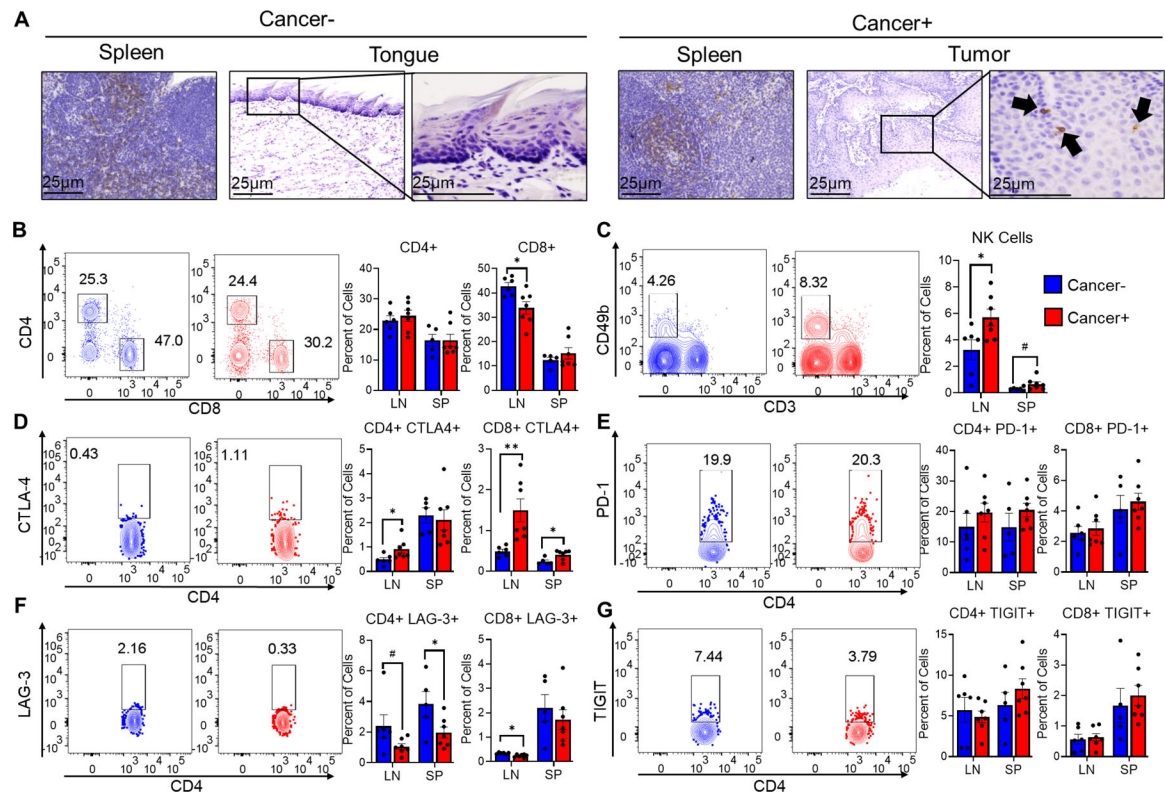
Figure 4. Lymphoid cell populations in HNSCC tumor bearing *Tgfβr1/Pten* 2cKO mice:
(A) Representative immunohistochemistry images of CD8 staining in spleen and tongue of
non tumor bearing mice (cancer-) and spleen and tumor of tumor bearing mice (cancer+).
Black arrows indicate the presence of positive stained cells in tumor images. **(B-C).**
Representative flow cytometry plots and graphs showing percentages of **(B)** CD4+, CD8+,
and (**C**) NK cells (CD3- CD49b+) in tumor draining lymph nodes (LN) and spleens (SP)
of tumor bearing (cancer+) and non tumor bearing (cancer-) *Tgfβr1/Pten* 2cKO mice **(D-G)**
Representative flow cytometry plots and graphs depicting percentages of **(D)** CTLA4+, **(E)**
PD-1+, **(F)** LAG-3+, and **(G)** TIGIT+ expressing CD4+ and CD8+ T cell populations in
lymph nodes (LN) and spleens (SP) of tumor bearing (cancer+) and non tumor bearing
(cancer-) *Tgfβr1/Pten* 2cKO mice. Data are presented as mean ± SE # *P*-value < 0.1, *
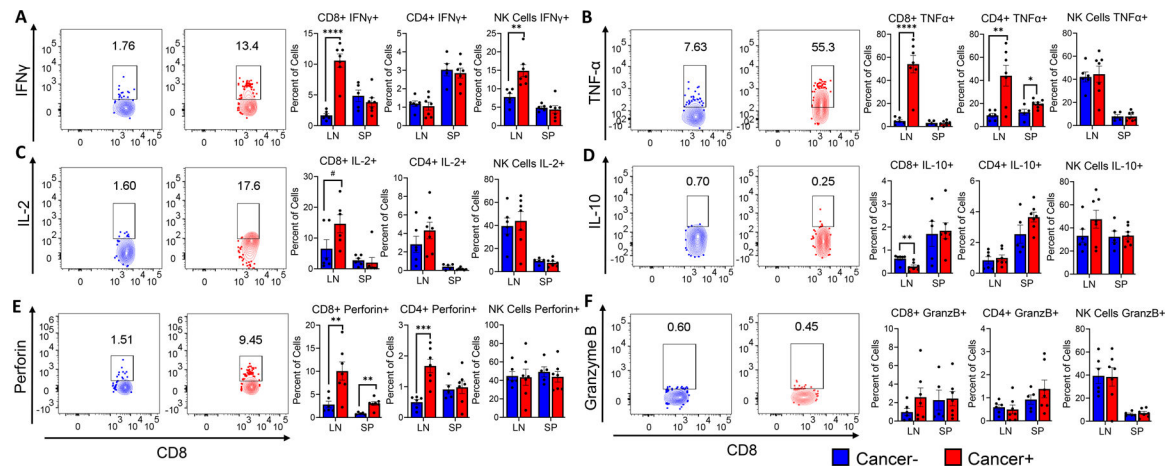*P*-value < 0.05; ** *P*-value < 0.01.

Figure 5: Cytokine, Perforin and Granzyme B production in lymphoid cell populations in HNSCC tumor bearing *Tgfβr1/Pten* 2cKO mice:

A-F. Representative flow cytometry plots and bar graphs showing average percentage of **(A)** IFNγ+, **(B)** TNF-α+, **(C)** IL-2+, (D) IL-10+, (E) perforin+, and (F) granzyme B+ producing CD8+, CD4+, and NK cell populations, in tumor draining lymph nodes (LN) and spleens (SP) of tumor bearing (cancer+) and non tumor bearing (cancer-) *Tgfβr1/Pten* 2cKO mice. Mouse groups include 6 tumor bearing mice and 7 non tumor bearing mice. Data are presented as mean ± SE # *P*-value < 0.1, * *P*-value < 0.05; ** *P*-value < 0.01; *** *P*-value <0.001.
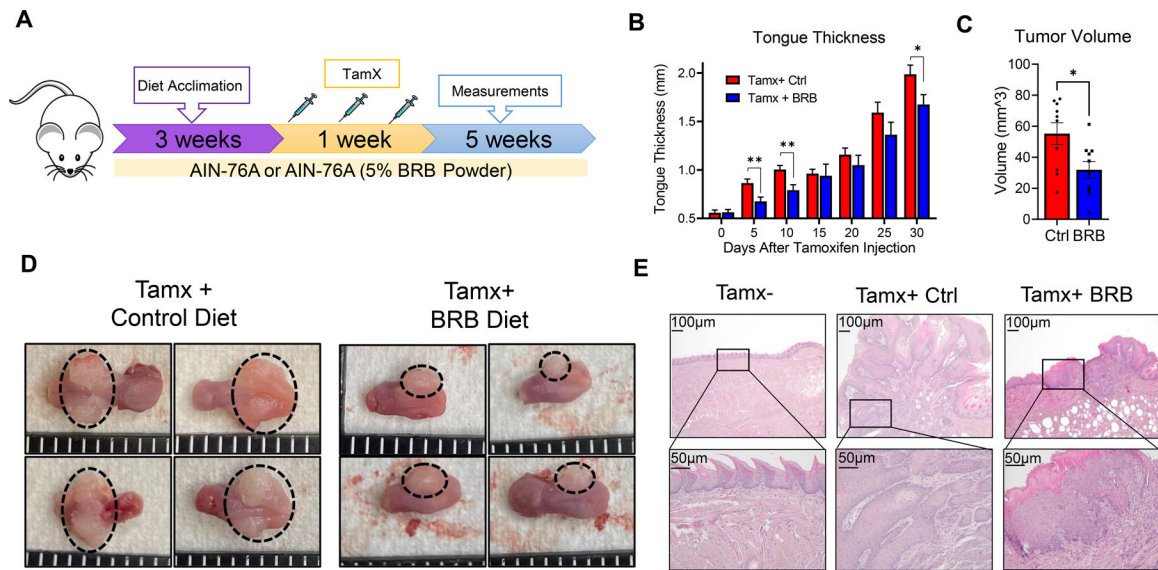
Figure 6: Black raspberry diet reduces HNSCC tumor burdens of mice with PTEN and TGFβ-R1 deletion:

(A) Schema of HNSCC induction and dietary chemoprevention with BRB in *Tgfβr1/Pten* 2cKO mice. Mice were fed control or BRB supplemented diet 3 weeks prior to HNSCC induction via intralingual tamoxifen injection and continued throughout the duration of the study. **(B)** Tumor progression in HNSCC induced *Tgfβr1/Pten* 2cKO mice fed control or BRB supplemented diet as determined by mouse tongue width measurements. **(C)** Tumor volumes in tongues of HNSCC induced *Tgfβr1/Pten* 2cKO mice fed control or BRB supplemented diet at terminal sacrifice. **(D)** Representative images of mouse tongues of HNSCC induced *Tgfβr1/Pten* 2cKO mice fed control or BRB supplemented diet. **(E)** Representative H&E-stained tongue images of control *Tgfβr1/Pten* 2cKO mice, HNSCC induced *Tgfβr1/Pten* 2cKO mice fed control or BRB supplemented diet. Normal tongues of control *Tgfβr1/Pten* 2cKO mice without tamoxifen injection (Tamx-) are also shown. Data are presented as mean ± SE * *P*-value < 0.05; ** *P*-value < 0.01.
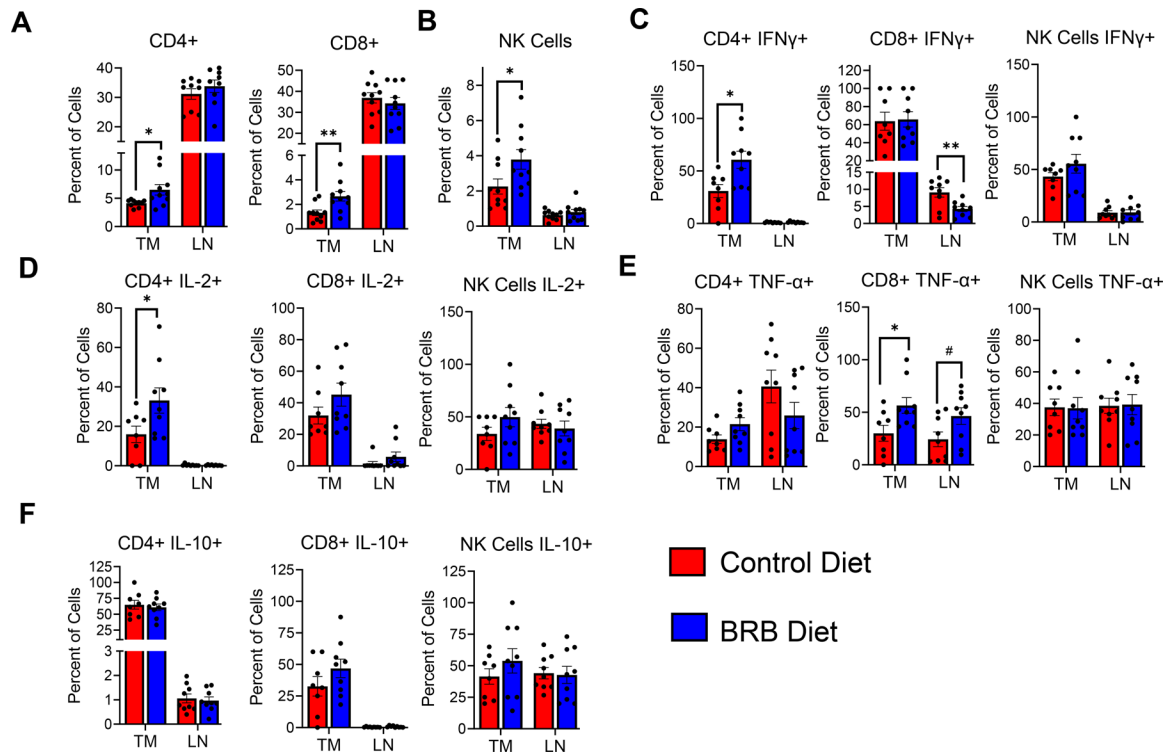
Figure 7: Dietary BRB administration promotes T cell infiltration to the tumor microenvironment:

(A-B) Representative flow cytometry plots and bar graphs depicting average percentage of **(A)** CD4+, CD8+ T cells, and **(B)** NK cells (CD3- CD49b+) in tumors (TM) and tumor draining lymph nodes (LN) of HNSCC induced *Tgfβr1/Pten* 2cKO mice fed control or BRB supplemented diet. **(C-F)** Representative flow cytometry plots and bar graphs showing average percentage of **(C)** IFNγ+, **(D)** IL-2+, **(E)** TNF-α+, and **(F)** IL-10+ producing CD4+, CD8+ T cells and NK cells, in tumors (TM) and tumor draining lymph nodes (LN) of HNSCC induced *Tgfβr1/Pten* 2cKO mice fed control or BRB supplemented diet. Data are presented as mean ± SE * *P*-value < 0.05; ** *P*-value < 0.01.
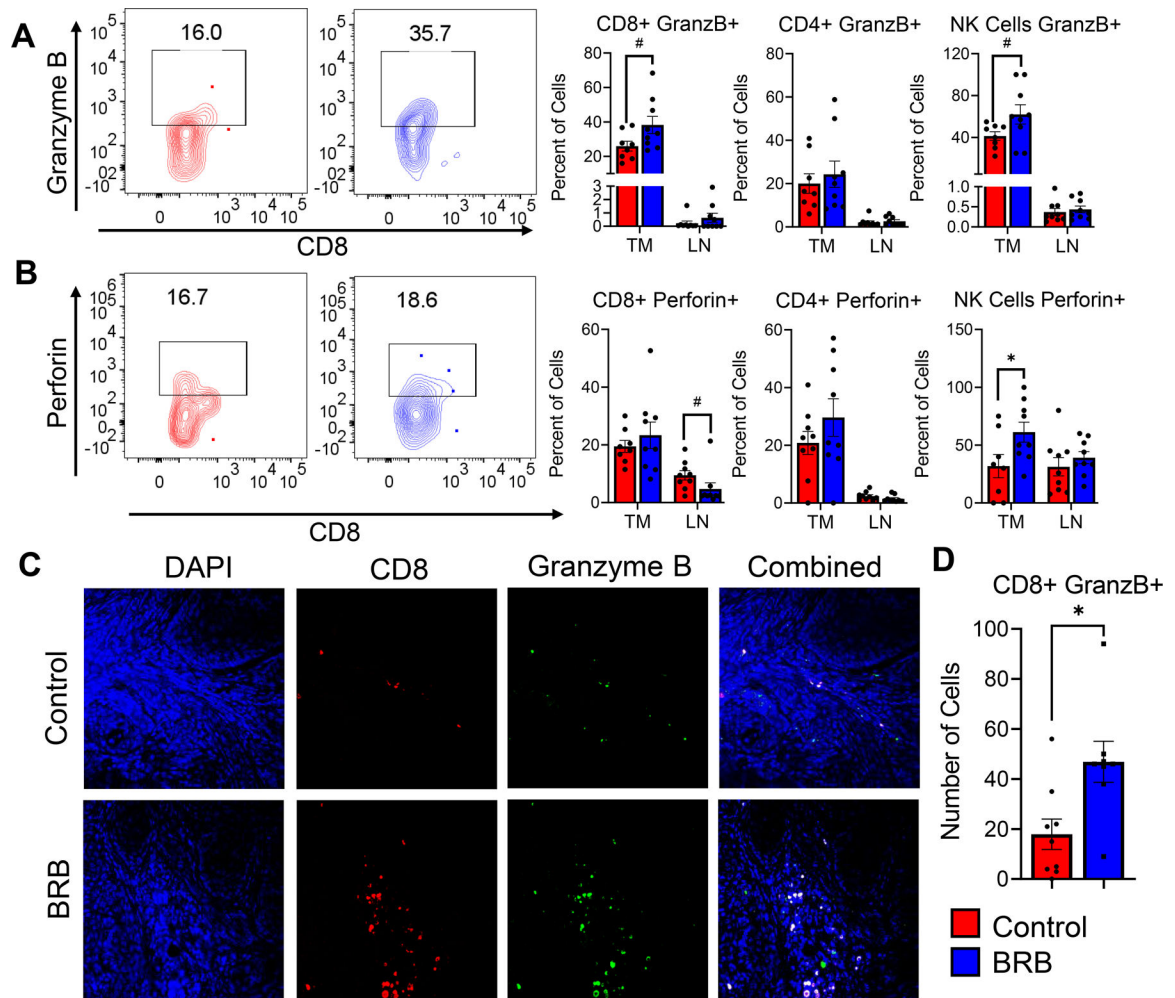
Figure 8: Dietary BRB administration stimulates anti-tumoral CD8+ cytotoxic T cell activity in HNSCC induced *Tgfβr1/Pten* 2cKO mice.

(A-B) Representative flow cytometry plots and bar graphs showing average percentage of (A) granzyme B, (B) perforin producing CD8+, CD4+ T cells, and NK cells in tumors (TM) and tumor draining lymph nodes (LN) of HNSCC induced *Tgfβr1/Pten* 2cKO mice fed control or BRB supplemented diet. (**C**) Representative immunofluorescence staining of tongue tumors of HNSCC induced *Tgfβr1/Pten* 2cKO mice fed control or BRB supplemented diet, Tissues were stained with DAPI (blue), CD8 (red), granzyme B (green). Composite image is also shown. **(D)** Bar graphs depicting average Granzyme B+ producing cells and Granzyme B producing CD8+ T cells based on immunofluorescence images. Quantification of graphical images were taken from at least three fields with N = 8–9 animals per group. Data are presented as mean ± SE # *P*-value < 0.1, * *P*-value < 0.05; ** *P*-value < 0.01.